

DiffMatch: Diffusion Model for Dense Matching

Jisu Nam Gyuseong Lee Sunwoo Kim Hyeonsu Kim
Hyoungwon Cho Seyeon Kim Seungryong Kim

Korea University

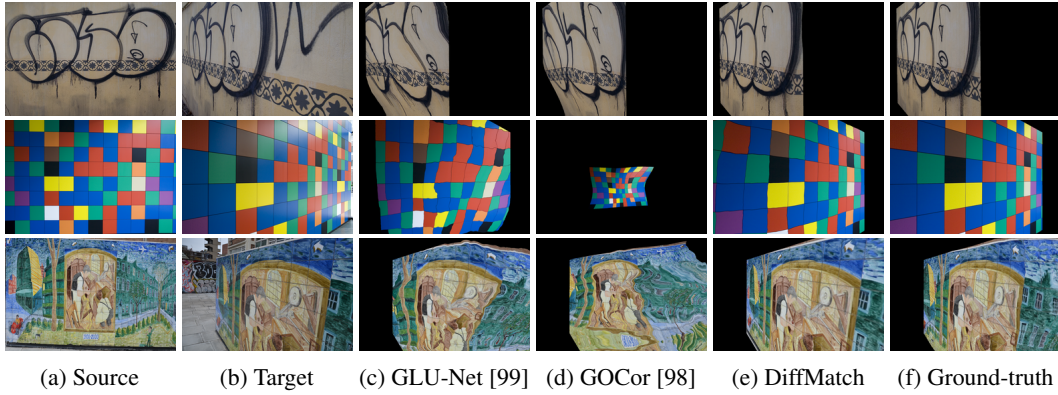


Figure 1: **Visualizing the effectiveness of the proposed DiffMatch:** (a) source images, (b) target images, and warped source images using estimated correspondences by (c-d) state-of-the-art approaches [99, 98], (e) our DiffMatch, and (f) ground-truth. Compared to previous methods [99, 98] that discriminatively estimate correspondences, our diffusion-based generative framework effectively learns the matching field manifold, resulting in better estimating correspondences particularly at textureless regions, repetitive patterns, and large displacements.

Abstract

The objective for establishing dense correspondence between paired images consists of two terms: a data term and a prior term. While conventional techniques focused on defining hand-designed prior terms, which are difficult to formulate, recent approaches have focused on learning the data term with deep neural networks without explicitly modeling the prior, assuming that the model itself has the capacity to learn an optimal prior from a large-scale dataset. The performance improvement was obvious, however, they often fail to address inherent ambiguities of matching, such as textureless regions, repetitive patterns, and large displacements. To address this, we propose DiffMatch, a novel conditional diffusion-based framework designed to explicitly model both the data and prior terms. Unlike previous approaches, this is accomplished by leveraging a conditional denoising diffusion model. DiffMatch consists of two main components: conditional denoising diffusion module and cost injection module. We stabilize the training process and reduce memory usage with a stage-wise training strategy. Furthermore, to boost performance, we introduce an inference technique that finds a better path to the accurate matching field. Our experimental results demonstrate significant performance improvements of our method over existing approaches, and the ablation studies validate our design choices along with the effectiveness of each component. Project page is available at <https://ku-cvlab.github.io/DiffMatch/>.

1 Introduction

Establishing pixel-wise correspondences between pairs of images has been one of the crucial problems, as it supports a wide range of applications, including structure from motion (SfM) [82], simultaneous localization and mapping (SLAM) [24, 2], image editing [5, 15, 106], and video analysis [36, 51]. In contrast to sparse correspondence [9, 57, 80] which detects and matches only a sparse set of key points, dense correspondence [71, 75, 45, 16] matches all the points between input images.

In the probabilistic interpretation, the objective for dense correspondence can be defined with the *data* term, measuring matching evidence between source and target features, and the *prior* term, encoding prior knowledge of correspondence. Traditional methods [71, 21, 104, 53, 55, 28] explicitly incorporated hand-designed prior terms to achieve smoother correspondence, such as total variation (TV) or discontinuity-aware smoothness. However, the formulation of the hand-crafted prior term is notoriously challenging and may vary depending on the specific dense correspondence task, such as geometric matching [55, 23, 44] or optical flow [103, 74].

Unlike them, recent approaches [46, 94, 75, 76, 99, 62, 45, 40, 16, 17] have focused on learning the data term with deep neural networks. However, despite demonstrating certain performance improvements [99, 98], these methods still struggle with effectively addressing the inherent ambiguities encountered in dense correspondence, including challenges posed by textureless regions, repetitive patterns, and large displacements. We argue that it is because they concentrate on maximizing the likelihood, which corresponds to learning the data term only, and do not explicitly consider matching priors. This limits their ability to learn the ground-truth matching field manifold and leads to poor generalization.

On the other hand, diffusion model [30, 89, 90, 91], one of the generative models, has recently proved the most powerful capability of learning posterior distribution and achieved considerable success among generative models [42]. Building on these advancements, recent studies have also focused on adding conditions in diffusion models [77, 84, 78, 77, 78, 59]. Furthermore, this progress has also led to the successful application in numerous discriminative tasks, such as depth estimation [81, 43, 22], object detection [11], segmentation [27, 25], and human pose estimation [31].

Inspired by the recent success of the diffusion model [30, 89, 90, 91], we introduce DiffMatch, a conditional diffusion-based framework designed to *explicitly* model the matching field distribution. Unlike existing discriminative learning-based methods [46, 40, 75, 76, 96] that focus solely on maximizing the likelihood, DiffMatch aims to learn the posterior distribution of dense correspondence given source and target features as conditions. Our framework mainly consists of two parts; conditional denoising diffusion module and cost injection module. The conditioning denoising diffusion module is designed to learn how to generate a correspondence field given feature descriptor and initial correspondence as conditions. To further boost the performance, we also adopt the cost injection module, which effectively inserts the pixel-wise matching confidences into the diffusion module. For stable convergence and efficient memory usage, we train conditional denoising diffusion module and cost injection module using stage-wise training. In the inference stage, we propose an inference strategy to find the best correspondence in the learned matching field distribution.

We evaluate the effectiveness of DiffMatch using several standard benchmarks [3, 83], and show the robustness of our model with the corrupted datasets [29, 3, 83]. We also conduct extensive ablation studies to validate our design choices and explore the effectiveness of each component.

2 Related work

Dense correspondence. Conventional techniques [34, 58] for dense correspondence have focused on formulating hand-designed matching priors. Some approaches [92, 7, 55, 95, 47, 28, 44] have introduced optimization techniques, such as SIFT Flow [55], which designed smoothness and small displacement priors, and DCTM [47] which proposed discontinuity aware prior term. However, manually constructing the prior is notoriously challenging. To address this issue, recent advances have adopted a learning paradigm [20, 75, 85, 61, 73, 96, 94, 99, 100, 40] that designs an objective function to solely maximize likelihood, assuming that an optimal matching prior can be learned within the network architecture on large-scale dataset. DGC-Net [61] and GLU-Net [99] proposed a coarse-to-fine framework with a feature pyramid, while COTR [40] introduced a transformer-based network.

GOCor [98] proposed a differentiable matching module that learns spatial priors to resolve matching ambiguities. Despite their success, these methods still face challenges in matching textureless regions, repetitive patterns, and large displacements, because of the lack of explicit awareness of the prior.

Diffusion models. Diffusion models [88, 30] have been largely researched due to their powerful generation capability. Denoising diffusion probabilistic models (DDPM) [30] proposed diffusion model where the forward and reverse processes exhibit the Markovian property. Denoising diffusion implicit models (DDIM) [89] accelerated DDPM by replacing the original diffusion process with non-Markovian chains to enhance sampling speed. On the other hand, conditional diffusion models have also been actively studied. Text-to-image generation models [67, 77, 79, 72] and image-to-image translation models [78] achieved surprising results. Meanwhile, recent works [105, 66] focusing on leveraging prior knowledge from large pretrained models, such as Stable Diffusion [77], have gained popularity for controlled generation by incorporating additional conditions. ControlNet [105] attached additional trainable copies of the diffusion model, while T2I-adapter [66] proposed lightweight adapters to inject guidance information.

Diffusion model for discriminative tasks. Recently, the remarkable performance of the diffusion model has been extended to solve discriminative tasks, including image segmentation [12, 27, 39], depth estimation [81, 43, 22, 39], object detection [11], and pose estimation [97, 31]. These approaches have demonstrated noticeable performance improvement using diffusion-based architecture. Our method represents the first application of the diffusion model to the dense correspondence task.

3 Preliminaries

Probabilistic interpretation of dense correspondence. Let us denote a pair of images, i.e., source and target, as I_{src} and I_{tgt} that represent visually or semantically similar images, and feature descriptors extracted from I_{src} and I_{tgt} as D_{src} and D_{tgt} , respectively. The objective of dense correspondence is to find a correspondence field F that is defined at each pixel i , which warps I_{src} towards I_{tgt} such that $I_{\text{tgt}}(i) \sim I_{\text{src}}(i + F(i))$ or $D_{\text{tgt}}(i) \sim D_{\text{src}}(i + F(i))$.

This objective can be formulated within probabilistic interpretation [86, 93, 28, 47], where we seek to find F^* that maximizes the posterior probability of the correspondence field given a pair of feature descriptors D_{src} and D_{tgt} , i.e., $p(F|D_{\text{src}}, D_{\text{tgt}})$. According to Bayes' theorem [41], the posterior can be decomposed such that $p(F|D_{\text{src}}, D_{\text{tgt}}) \propto p(D_{\text{src}}, D_{\text{tgt}}|F) \cdot p(F)$. To find the matching field F^* that maximizes the posterior, we can use the maximum a posteriori (MAP) approach [26]:

$$\begin{aligned} F^* &= \underset{F}{\operatorname{argmax}} p(F|D_{\text{src}}, D_{\text{tgt}}) = \underset{F}{\operatorname{argmax}} p(D_{\text{src}}, D_{\text{tgt}}|F) \cdot p(F) \\ &= \underset{F}{\operatorname{argmax}} \underbrace{\{\log p(D_{\text{src}}, D_{\text{tgt}}|F) + \log p(F)\}}_{\text{data term}} \underbrace{\{\log p(F)\}}_{\text{prior term}}. \end{aligned} \quad (1)$$

In this probabilistic interpretation, the first term, referred to as *data* term, represents the matching evidence between feature descriptors D_{src} and D_{tgt} , and the second term, referred to as *prior* term, encodes prior knowledge of the matching field F .

Denoising diffusion models. The diffusion model is a type of generative model, and can be divided into two categories: unconditional models [88, 30] and conditional models [6, 19]. Specifically, unconditional diffusion models learn an explicit approximation of the data distribution, denoted as $p(X)$. On the other hand, conditional diffusion models estimate the data distribution given a certain condition K , e.g., text prompt [19], denoted as $p(X|K)$.

In the conditional diffusion model, the data distribution is approximated by recovering a data sample from the Gaussian noise through an iterative denoising process. Given a sample X_0 , it is transformed to X_t through the forward diffusion process at a time step $t \in \{T, T-1, \dots, 1\}$, which consists of Gaussian transition at each time step $q(X_t|X_{t-1}) := \mathcal{N}(\sqrt{1-\beta_t}X_{t-1}, \beta_t I)$. The forward diffusion process follows the pre-defined variance schedule β_t such that

$$X_t = \sqrt{\alpha_t}X_0 + \sqrt{1-\alpha_t}Z, \quad Z \sim \mathcal{N}(0, I), \quad (2)$$

where $\alpha_t = \prod_{i=1}^t (1 - \beta_i)$. After training, we can sample data from the learned distribution through iterative denoising with the pre-defined range of time steps, called the reverse diffusion process following the non-Markovian process of DDIM [89], which is parametrized as another Gaussian

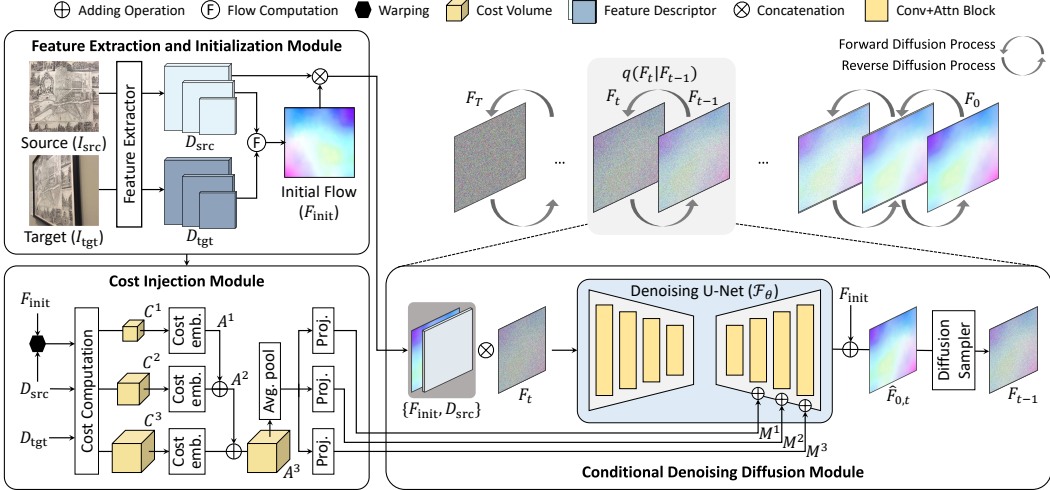


Figure 2: **Overall network architecture of DiffMatch.** Our network consists of two key components: a conditional denoising diffusion module that generates the matching fields based on the conditions, and a cost injection module that embeds further pixel-wise interactions among paired source and target images into the diffusion module.

transition $p_\theta(X_{t-1} | X_t) := \mathcal{N}(X_{t-1}; \mu_\theta(X_t, t), \sigma_\theta(X_t, t)\mathbf{I})$. To this end, the diffusion network $\mathcal{F}_\theta(X_t, t; K)$ predicts the denoised sample $\hat{X}_{0,t}$ given X_t , t and K . One step in the reverse diffusion process can be formulated such that

$$X_{t-1} = \sqrt{\alpha_{t-1}} \mathcal{F}_\theta(X_t, t; K) + \frac{\sqrt{1 - \alpha_{t-1} - \sigma_t^2}}{\sqrt{1 - \alpha_t}} \left(X_t - \sqrt{\alpha_t} \mathcal{F}_\theta(X_t, t; K) \right) + \sigma_t Z \quad (3)$$

where σ_t is the covariance value of Gaussian distribution at time step t .

The iterative denoising process can be viewed as finding $X^* = \text{argmax}_X \log p(X|K)$ through the relationship between the conditional sampling process of DDIM [89] and conditional score-based generative models [6].

4 Methodology

4.1 Motivation

Recent learning-based methods [46, 94, 75, 76, 99, 62, 45, 40, 16, 17] have employed deep neural networks $\mathcal{F}(\cdot)$ to directly approximate the *data* term, i.e., $\text{argmax}_F \log p(D_{\text{src}}, D_{\text{tgt}}|F)$, without explicitly considering *prior* term. For instance, GLU-Net [99] and GOCor [98] construct a cost volume along candidates F between source and target features D_{src} and D_{tgt} , and regresses the matching fields F^* within neural networks, which might be analogy to $\text{argmax}_F \log p(D_{\text{src}}, D_{\text{tgt}}|F)$. In this setting, dense correspondence F^* is estimated as follows:

$$F^* = \mathcal{F}_\theta(D_{\text{src}}, D_{\text{tgt}}) \approx \text{argmax}_F \underbrace{\log p(D_{\text{src}}, D_{\text{tgt}}|F)}_{\text{data term}}, \quad (4)$$

where $\mathcal{F}_\theta(\cdot)$ and θ represent a feed-forward network and its parameters, respectively. These approaches assume that the matching prior can be learned within the model architecture by leveraging the high capacity of deep networks [99, 40, 16, 17, 62] and the availability of large-scale datasets. While there is obvious performance improvement, they typically focus on the data term without explicitly considering the matching prior. This can restrict ability of the model to learn the manifold of matching field and result in poor generalization.

4.2 Formulation

To address these limitations, for the first time, we explore a conditional generative model for dense correspondence to explicitly learn both the *data* and *prior* terms. Unlike previous discriminative

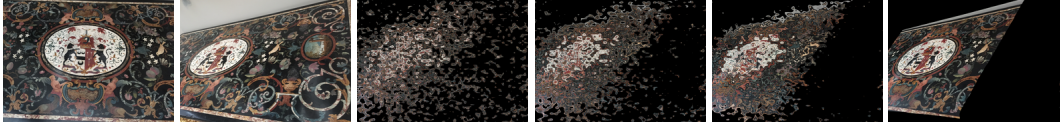


Figure 3: **Visualization of the reverse diffusion process:** (from left to right) source and target images, and warped source images by estimated correspondences as evolving time steps. The source image is progressively warped into the target image through an iterative denoising process.

learning-based approaches [71, 21, 104, 46, 94, 75], we achieve this by leveraging a conditional generative model that jointly learns the data and prior through optimization of the following objective:

$$\begin{aligned} F^* &= \mathcal{F}_\theta(D_{\text{src}}, D_{\text{tgt}}) \approx \operatorname{argmax}_F p(F|D_{\text{src}}, D_{\text{tgt}}) \\ &= \operatorname{argmax}_F \underbrace{\{\log p(D_{\text{src}}, D_{\text{tgt}}|F)\}}_{\text{data term}} + \underbrace{\{\log p(F)\}}_{\text{prior term}}. \end{aligned} \quad (5)$$

Inspired by the recent success of diffusion models [88, 30, 68, 19, 79, 77], we employ the conditional diffusion process [6, 19] to *explicitly* learn $\operatorname{argmax}_F p(F|D_{\text{src}}, D_{\text{tgt}})$. We leverage the capacity of a conditional diffusion model, which generates high-fidelity and diverse samples aligned with the given conditions, to search for accurate matching within the learned correspondence manifold.

Specifically, we define the forward diffusion process for dense correspondence as the Gaussian transition such that $q(F_t|F_{t-1}) := \mathcal{N}(\sqrt{1-\beta_t}F_{t-1}, \beta_t I)$, where β_t is a predefined variance schedule. The resulting latent variable F_t can be formulated as Eq. (2):

$$F_t = \sqrt{\alpha_t}F_0 + \sqrt{1-\alpha_t}Z, \quad Z \sim \mathcal{N}(0, I), \quad (6)$$

where F_0 is the ground-truth correspondence. In addition, the neural network $\mathcal{F}_\theta(\cdot)$ is subsequently trained to reverse the forward diffusion process. During the reverse diffusion phase, the initial latent variable F_T is iteratively denoised following the sequence $F_{T-1}, F_{T-2}, \dots, F_0$, using Equation (3):

$$F_{t-1} = \sqrt{\alpha_{t-1}}\mathcal{F}_\theta(X_t, t; D_{\text{src}}, D_{\text{tgt}}) + \frac{\sqrt{1-\alpha_{t-1}-\sigma_t^2}}{\sqrt{1-\alpha_t}} \left(X_t - \sqrt{\alpha_t}\mathcal{F}_\theta(F_t, t; D_{\text{src}}, D_{\text{tgt}}) \right) + \sigma_t Z, \quad (7)$$

where $\mathcal{F}_\theta(F_t, t; D_{\text{src}}, D_{\text{tgt}})$ directly predicts the denoised correspondence $\hat{F}_{0,t}$ with source and target features, D_{src} and D_{tgt} , as conditions.

The objective of this denoising process is to find the optimal correspondence field F^* that satisfies $\operatorname{argmax}_F \log p(F|D_{\text{src}}, D_{\text{tgt}})$. The detailed explanation of the objective function of the denoising process will be explained in the Sec. 4.4.

4.3 Network architecture

In this section, we discuss how to design the network architecture $\mathcal{F}_\theta(\cdot)$. Our goal is to find accurate matching fields given feature descriptors D_{src} and D_{tgt} from I_{src} and I_{tgt} , respectively, as conditions. An overview of our proposed architecture is provided in Fig. 2.

Cost computation. Following conventional methods [76, 98], we compute the matching cost that calculates pairwise cosine similarity scores between all locations in the feature descriptors, formulated as follows:

$$C(i, j) = \frac{D_{\text{src}}(i) \cdot D_{\text{tgt}}(j)}{\|D_{\text{src}}(i)\| \|D_{\text{tgt}}(j)\|}, \quad (8)$$

where $i \in [0, h_{\text{src}}) \times [0, w_{\text{src}})$, $j \in [0, h_{\text{tgt}}) \times [0, w_{\text{tgt}})$, and $\|\cdot\|$ denotes $l\text{-}2$ normalization.

Conditional denoising diffusion module. As illustrated in Fig. 2, to train diffusion models, we present a modified U-Net architecture based on [68]. Since correspondences often exhibit consistency for semantically related regions in the source image [94, 35], we take the source feature D_{src} as another input with the noisy input correspondence F_t . Furthermore, we compel the networks to learn the residual of initially estimated correspondence to stabilize the learning process and provide a better initialization. Specifically, we derive the initial correspondence F_{init} using the soft-argmax

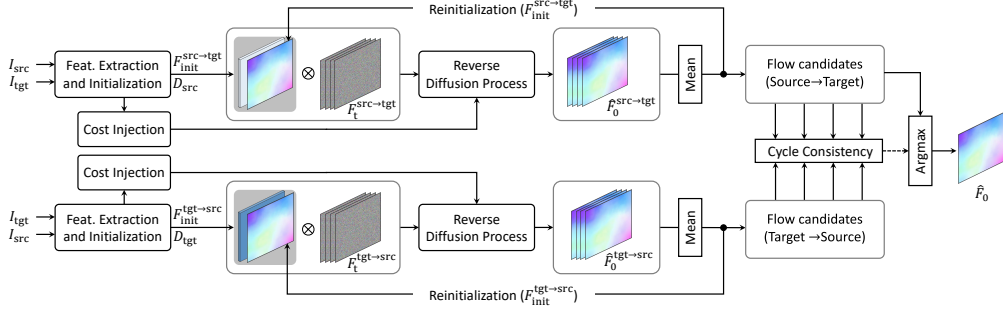


Figure 4: **Illustration of the proposed inference technique.** To stabilize the reverse diffusion process, we measure the mean of estimated multiple matching flows from different initializations. We iteratively reinitialize the initial matching field with the previously estimated one. Subsequently, we find the most confident estimated match among the flow candidates through cycle consistency.

operation [16] on the matching cost C between D_{src} and D_{tgt} . We then take F_{init} as an additional condition with F_t and D_{src} . We also add F_{init} to the output of the network.

Cost injection module. We further introduce cost injection module, which improves the discriminative power of the matching cost by further integrating pixel-wise interactions between paired images into the denoising U-Net. As illustrated in the left bottom part of Fig. 2, it consists of two main components: cost embedding blocks and projection layers. Previous studies [61, 99, 64, 65] have shown that utilizing multi-level features allows the model to capture hierarchical semantic feature representations. Inspired by [63, 17], for each l -th level of feature resolution, we compute a correlation map C^l similar to Eq. (8) between warped source feature descriptors $D_{src \rightarrow tgt}^l$ and $D_{tgt \rightarrow tgt}^l$, where $D_{src \rightarrow tgt}^l$ is obtained by warping D_{src}^l with F_{init} to further account for residual error of F_{init} . The correlation maps at each level are subsequently fed into the cost embedding block to produce locally aggregated volume A^l . Specifically, the cost embedding block consists of 4D convolutions, Group Normalization, and ReLU operations sequentially. In addition, we incorporate multi-level correlation maps by adding the embedded correlation map of the previous level A^{l-1} to A^l . Concretely, A^{l-1} is upsampled using bilinear upsampling and then passed through a 4D convolutional layer, which is denoted as $up(A^{l-1})$ as follows: $A^l = A^l + up(A^{l-1})$ for $l \in [1, L]$.

The final embedded correlation map A^L at level L is compressed by average pooling across the last two target dimensions, resulting in a 2-dimensional representation. The average-pooled feature map is then passed through corresponding 2D convolutional projection layers with bilinear interpolation for alignment with the intermediate features U in the denoising U-Net decoder of $\mathcal{F}_\theta(\cdot)$. Finally, the projection of the embedded correlation map M^n is added to corresponding n -th layer U^n at each level of decoder as follows: $\hat{U}^n = U^n + M^n$ for $n \in [1, N]$.

4.4 Stage-wise training

The most straightforward approach to train our architecture is through end-to-end learning [22, 81, 11, 27, 31, 99, 98]. However, it may yield suboptimal performance since the networks need to simultaneously learn the prior and precisely find matching field by fully exploiting the given features as conditions. To overcome this, we propose a stage-wise training method that allows accurate control over the generation process while fully leveraging the prior knowledge learned by the model. This approach is inspired by recent studies [105, 14, 66] that successfully control pretrained diffusion models using task-specific conditions.

Training diffusion prior for dense correspondence. In the first stage, the denoising U-Net, as illustrated in Sec. 4.3, learns the prior knowledge of the matching field with the initial correspondence F_{init} to give a matching hint and the source feature D_{src} to provide a structural hint. In other words, we redefine the network $\mathcal{F}_\theta(F_t, t; D_{src}, D_{tgt})$ as $\mathcal{F}_\theta(F_t, t; D_{src}, F_{init})$, given that F_{init} is derived from D_{src} and D_{tgt} as described in Sec. 4.3. In the first stage, the loss function is defined as follows:

$$\mathcal{L}_{\text{stage-1}} = \mathbb{E}_{F_0, t, Z \sim \mathcal{N}(0, I)} \left[\|F_0 - \mathcal{F}_\theta(F_t, t; D_{src}, F_{init})\|^2 \right]. \quad (9)$$

Injecting cost information. In the second stage, we use additional pixel-wise interactions between paired images as extra guidance to control the learned prior. Specifically, we freeze all the parameters

of the denoising U-Net learned in the first stage, and only train a compact cost injector module, detailed in Sec. 4.3. This allows the cost injector module to leverage the learned generative prior, aligning the internal prior knowledge in U-Net with the external matching cost. In the second stage, we redefine the neural network $\mathcal{F}_\theta(F_t, t; D_{\text{src}}, F_{\text{init}})$ as $\mathcal{F}_\theta(F_t, t; D_{\text{src}}, F_{\text{init}}, M)$, where M is the cost derived by cost injection module. The loss function in the second stage is defined as follows:

$$\mathcal{L}_{\text{stage-2}} = \mathbb{E}_{F_0, t, Z \sim \mathcal{N}(0, I)} \left[\|F_0 - \mathcal{F}_\theta(F_t, t; D_{\text{src}}, F_{\text{init}}, M)\|^2 \right]. \quad (10)$$

Note that connecting our cost injection module is computationally efficient: with the original weights in diffusion model locked, no gradient computation on the original U-Net is required during training. We thoroughly assess the multi-stage learning in Table 4.

4.5 Inference

During the inference phase, a Gaussian noise F_T is gradually denoised into a more accurate matching field F_0 under the given features D_{src} and D_{tgt} as conditions through the diffusion reverse process, as visualized in Fig. 3. In the following section, we further discuss the application of our functional approach during inference to achieve more precise correspondences. The overall procedure of the proposed inference technique is illustrated in Fig. 4.

Multiple hypotheses. To account for the stochastic nature of diffusion-based models, we propose utilizing multiple hypotheses by computing the mean of the estimated multiple matching fields from multiple initializations F_T , as illustrated in Fig. 4, which helps to reduce stochasticity of model while improving the matching performance.

Recursive reinitialization. In cases where F_{init} is substantially erroneous, it may not be an ideal starting point. To address this, as illustrated in Fig. 4, we propose a recursive reinitialization strategy which iteratively replaces the initial matching field F_{init} with a previously estimated one. Specifically, if cycle consistency error [4] exceeds predefined threshold, we iteratively update F_{init} . This enables the network to find an improved starting point and a more effective path towards an ideal matching.

Discarding erroneous matches via cycle consistency. We further propose to discard erroneous matches after recursion, based on cycle consistency. Specifically, as depicted in Fig. 4, we employ a bi-directional two-way sampling method. In one direction, we estimate the source-to-target matches $\hat{F}_0^{\text{src} \rightarrow \text{tgt}}$ from the noise $F_T^{\text{src} \rightarrow \text{tgt}}$ given an initial correspondence $F_{\text{init}}^{\text{src} \rightarrow \text{tgt}}$. In the other direction, we estimate the target-to-source matches $\hat{F}_0^{\text{tgt} \rightarrow \text{src}}$, vice versa. During each iteration, we save predictions at each step of recursion and select the most confident matches based on cycle consistency at the end of the iterative process. This approach helps filter out erroneous cases arising from our proposed reinitialization, leading to a significant performance improvement, as shown in Table 5.

5 Experiments

5.1 Implementation details

For the feature extractor backbone, we used VGG-16 [10] and kept all parameters frozen throughout all experiments. Our diffusion network is based on [68] with modifications to the channel dimension. The network was implemented using PyTorch [70] and trained with the AdamW optimizer [56] at a learning rate of $1e^{-4}$ in the first stage and $3e^{-5}$ in the second stage. We conducted comprehensive experiments in geometric matching for two datasets: HPatches [3] and ETH3D [83]. For evaluation on HPatches, we trained our network using the self-supervised training procedure from [99] on the DPED-CityScape-ADE [38, 18, 107], and for evaluation on ETH3D, we used COCO-augmented DPED-CityScape-ADE [54] following [98]. We further highlight the effectiveness of our generative prior by evaluating our method against a set of common visual corruptions introduced in [29]. Further details, such as experimental settings about datasets [3, 83], can be found in the supplementary materials.

5.2 Matching results

HPatches. We evaluated DiffMatch on five viewpoints using standard evaluation metrics AEPE and PCK. Table 1 summarizes the quantitative results, demonstrating that our method surpasses

Table 1: **Quantitative evaluation on HPatches [3] and ETH3D [83]**. Lower AEPE indicates better performance. Higher scene labels or rates (e.g., V or 15) comprise more challenging images with extreme geometric deformations. The best results are highlighted in bold, and the second-best results are underlined. *: COTR [40] is examined separately since it provides only confident correspondences and evaluation is limited to this subset. †: This indicates that a dense evaluation is performed without zoom-in techniques and confidence thresholding for a fair comparison.

Methods	HPatches Original [3]							ETH3D [83]							
	I	II	III	IV	V	Avg.	5px	rate=3	rate=5	rate=7	rate=9	rate=11	rate=13	rate=15	Avg.
COTR* [40]	-	-	-	-	-	7.75	91.10	1.66	1.82	1.97	2.13	2.27	2.41	2.61	2.12
COTR*+Interp. [40]	-	-	-	-	-	7.98	86.33	1.71	1.92	2.16	2.47	2.85	3.23	3.76	2.59
DGC-Net [61]	5.71	20.48	34.15	43.94	62.01	33.26	58.06	2.49	3.28	4.18	5.35	6.78	9.02	12.25	6.19
GLU-Net [99]	<u>1.55</u>	12.66	27.54	32.04	52.47	25.05	78.54	<u>1.98</u>	<u>2.54</u>	<u>3.49</u>	4.24	5.61	7.55	10.78	5.17
GLU-Net-GOCor [98]	1.29	<u>10.07</u>	23.86	27.17	38.41	<u>20.16</u>	<u>81.43</u>	1.93	<u>2.28</u>	2.64	3.01	3.62	4.79	7.80	3.72
DMP [32]	3.21	15.54	32.54	38.62	63.43	30.64	63.21	2.43	3.31	4.41	5.56	6.93	9.55	14.20	6.62
COTR† [40]	19.65	33.81	45.81	62.03	66.28	45.52	5.10	8.76	9.86	11.23	12.44	13.77	14.94	16.09	12.44
DiffMatch	1.65	9.50	22.26	26.95	36.07	19.29	82.65	3.49	3.56	3.80	4.14	4.58	5.18	6.20	4.42



Figure 5: **Qualitative results on HPatches [3]**: the source images are warped to the target images using predicted correspondences.

state-of-the-art discriminative learning-based methods [99, 98]. The qualitative result is presented in Fig. 5. The effectiveness of our approach is evident from the quantitative results in Fig. 1. This success can be attributed to the robust generative prior that learns a matching field manifold, which effectively addresses challenges faced by previous discriminative methods, such as textureless regions, repetitive patterns, and large displacements.

ETH3D. As indicated in Table 1, our method achieves highly competitive performance compared to state-of-the-art discriminative learning-based methods and significantly surpasses them at an interval rate of 15, representing the most challenging settings. However, in ETH3D, the displacement is relatively small compared to HPatches, leading to saturated performance that does not align with our objective of developing a robust matching prior for addressing inherent challenges and ambiguities in dense correspondence. To more thoroughly evaluate the effectiveness and robustness of our generative prior, we conducted additional evaluations on common corruptions introduced in [29].

Robustness on corrupted datasets. In practical dense correspondence settings, corruptions such as weather variations or photographic distortions may occur. Therefore, finding robust dense correspondence in corrupted settings is crucial. However, previous discriminative approaches [99, 98] rely solely on the correlation layer, which compares only point-to-point feature relationships, resulting in degraded performance in harsh-corrupted settings. In contrast, our framework learns not only the likelihood but also the prior knowledge of the matching field formation.

To evaluate the robustness of the learned prior, we compare DiffMatch with other methods [99, 98] on corrupted settings [29] of HPatches and ETH3D. As shown in Table 3, our method exhibits outstanding performance in harsh corruptions, especially in blur and weather corruptions. Additionally, our superior performance is visually evident in Fig. 6.

Table 2: **Results via different learning schemes.**

Learning schemes	HPatches AEPE ↓	ETH3D AEPE ↓
DiffMatch w/o diffusion	23.75	5.57
DiffMatch	19.29	4.42

5.3 Ablation study

Effectiveness of generative prior. We aim to validate our hypothesis that a diffusion-based generative prior is effective for finding a more accurate matching field. To achieve this, we train our network by directly regressing the matching field. Then we compare its performance with our diffusion-based method. As demonstrated in Table 2, our generative approach outperforms the regression-based baseline, thereby emphasizing the efficacy of the generative prior in dense correspondence tasks.

Table 3: **Quantitative evaluation on HPatches [3] and ETH3D [83] with common corruptions from ImageNet-C [29].** All results are evaluated at corruption severity 5. For simplicity, we denote GLU-Net-GOCor as GOCor [98].

Dataset	Algorithm	Gauss.	Noise Shot	Impulse	Defocus	Blur Glass	Motion	Zoom	Snow	Frost	Weather Fog	Bright	Contrast	Digital Elastic	Pixel	JPEG	Avg.
HPatches [3]	GLU-Net [99]	34.96	32.60	34.18	25.74	25.71	63.26	90.75	46.16	66.63	47.81	25.28	37.45	32.85	44.31	26.94	42.31
	GOCor [98]	27.35	27.21	26.63	23.54	20.75	57.75	88.35	39.84	63.55	36.98	21.44	23.65	28.40	33.67	22.20	36.09
	DiffMatch	30.82	29.18	29.73	21.76	19.21	56.87	95.06	35.48	48.24	31.10	19.33	27.41	28.00	35.57	23.68	35.42
ETH3D [83]	GLU-Net [99]	29.20	27.51	29.11	14.18	13.16	36.90	77.73	47.11	65.22	37.75	13.89	24.52	19.11	21.25	17.77	31.63
	GOCor [98]	27.45	25.56	26.44	11.39	10.98	33.73	73.56	43.24	66.49	39.11	10.98	18.34	15.54	16.47	15.20	28.96
	DiffMatch	26.40	23.63	26.17	8.82	7.66	34.01	69.30	38.99	64.82	26.93	10.04	15.17	13.89	17.37	15.39	26.57



Figure 6: **Qualitative results on ETH3D [83] using Fog corruption in [29]:** the source images are warped to the target images using predicted correspondences.

Trade-off between sampling time steps and accuracy. Fig. 7 illustrates the trade-off between sampling time steps and matching accuracy. As the sampling time steps increase, the matching performance progressively improves in our framework. After time step 5, it outperforms all other existing methods [99, 98, 37, 94, 32], and the performance also converges. In comparison, DMP [32], which optimizes the neural network to learn the matching prior of an image pair at test time, requires approximately 300 steps. These results highlight that DiffMatch finds a shorter and better path to accurate matches in relatively fewer steps during the inference phase.

Component analysis. In this ablation study, we aim to provide a quantitative comparison between different training strategies. Table 4 summarizes the results: **(I)** refers to end-to-end training of the entire architecture shown in Fig. 2. **(II)** denotes stage 1, where the conditional denoising diffusion module is trained. **(III)** represents stage 2, in which only the cost injection module is trained while the denoising diffusion module remains frozen. **(III)** outperforms **(II)**, highlighting the effectiveness of the cost injection module and memory efficiency of our stage-wise training strategy. In addition, we can find that stage-wise training is more stable than end-to-end training.

Inference strategies. In this ablation study, we quantitatively ablate the components of the proposed inference strategy. \ddagger indicates the corrupted settings. The results are presented in Table 5. **(I)** indicates the default reverse sampling, while **(II)**, **(III)**, and **(IV)** represent multiple hypotheses, the recursive reinitialization technique, and cycle consistency in Sec. 4.5, respectively. **(II)** demonstrates that multiple hypotheses stabilize the reverse diffusion process, while **(III)** and **(IV)** contribute to identifying better starting points and filtering out erroneous cases through cycle consistency.

6 Conclusion

In this paper, we propose a novel diffusion-based framework for dense correspondence, named DiffMatch, which jointly models the likelihood and prior distribution of the matching fields. The proposed framework mainly consists of the conditional denoising diffusion module and cost injection module. For stable convergence and efficient memory usage, we train the network in a stage-wise manner. To further boost performance, we propose an inference strategy to find the best

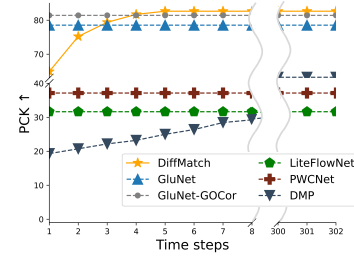


Figure 7: **Time steps vs. PCK.**

Table 4: **Ablations on components.**

	Components	HPatches AEPE \downarrow	ETH3D AEPE \downarrow	Memory [GB]
(I)	End-to-end training	24.56	6.07	3.02
(II)	Conditional denoising diff.	20.06	4.67	2.88
(III)	Frozen (II) + cost inject. (DiffMatch)	19.29	4.42	1.93

Table 5: **Ablations on inference strategy.**

	Components	HPatches AEPE \downarrow	\ddagger ETH3D AEPE \downarrow
(I)	Reverse diffusion process	$20.23 \pm 1e^{-3}$	$27.96 \pm 6e^{-2}$
(II)	(I) + Multiple hypotheses	20.23	27.96
(III)	(II) + Recursive reinit.	21.47	29.91
(IV)	(III) + Cycle consistency	19.29	26.57

correspondence in the learned matching field distribution. For the first time, we highlight the power of generative prior in dense correspondence, achieving state-of-the-art performance on standard benchmarks. We further emphasize the effectiveness of our generative prior in harshly corrupted settings of the benchmarks. As a result, we show that our diffusion-based generative approach significantly outperforms discriminative approaches in addressing inherent ambiguities present in dense correspondence.

References

- [1] Julien Abi-Nahed, Marie-Pierre Jolly, and Guang-Zhong Yang. Robust active shape models: A robust, generic and simple automatic segmentation tool. In *Medical Image Computing and Computer-Assisted Intervention—MICCAI 2006: 9th International Conference, Copenhagen, Denmark, October 1-6, 2006. Proceedings, Part II 9*, pages 1–8. Springer, 2006.
- [2] Tim Bailey and Hugh Durrant-Whyte. Simultaneous localization and mapping (slam): Part ii. *IEEE robotics & automation magazine*, 13(3):108–117, 2006.
- [3] Vassileios Balntas, Karel Lenc, Andrea Vedaldi, and Krystian Mikolajczyk. Hpatches: A benchmark and evaluation of handcrafted and learned local descriptors. In *Proceedings of the IEEE conference on computer vision and pattern recognition*, pages 5173–5182, 2017.
- [4] Daniel Barath, Jiri Matas, and Jana Noskova. Magsac: marginalizing sample consensus. In *Proceedings of the IEEE/CVF conference on computer vision and pattern recognition*, pages 10197–10205, 2019.
- [5] Connelly Barnes, Eli Shechtman, Adam Finkelstein, and Dan B Goldman. Patchmatch: A randomized correspondence algorithm for structural image editing. *ACM Trans. Graph.*, 28(3):24, 2009.
- [6] Georgios Batzolos, Jan Stanczuk, Carola-Bibiane Schönlieb, and Christian Etmann. Conditional image generation with score-based diffusion models. *arXiv preprint arXiv:2111.13606*, 2021.
- [7] Thomas Brox and Jitendra Malik. Large displacement optical flow: descriptor matching in variational motion estimation. *IEEE transactions on pattern analysis and machine intelligence*, 33(3):500–513, 2010.
- [8] Andrés Bruhn and Joachim Weickert. A confidence measure for variational optic flow methods. *Computational Imaging and Vision*, 31:283, 2006.
- [9] Michael Calonder, Vincent Lepetit, Christoph Strecha, and Pascal Fua. Brief: Binary robust independent elementary features. In *Computer Vision—ECCV 2010: 11th European Conference on Computer Vision, Heraklion, Crete, Greece, September 5-11, 2010, Proceedings, Part IV 11*, pages 778–792. Springer, 2010.
- [10] Ken Chatfield, Karen Simonyan, Andrea Vedaldi, and Andrew Zisserman. Return of the devil in the details: Delving deep into convolutional nets. *arXiv preprint arXiv:1405.3531*, 2014.
- [11] Shoufa Chen, Peize Sun, Yibing Song, and Ping Luo. Diffusiondet: Diffusion model for object detection. *arXiv preprint arXiv:2211.09788*, 2022.
- [12] Ting Chen, Lala Li, Saurabh Saxena, Geoffrey Hinton, and David J Fleet. A generalist framework for panoptic segmentation of images and videos. *arXiv preprint arXiv:2210.06366*, 2022.
- [13] Xiaozhi Chen, Kaustav Kundu, Ziyu Zhang, Huimin Ma, Sanja Fidler, and Raquel Urtasun. Monocular 3d object detection for autonomous driving. In *Proceedings of the IEEE conference on computer vision and pattern recognition*, pages 2147–2156, 2016.
- [14] Zhe Chen, Yuchen Duan, Wenhui Wang, Junjun He, Tong Lu, Jifeng Dai, and Yu Qiao. Vision transformer adapter for dense predictions. *arXiv preprint arXiv:2205.08534*, 2022.
- [15] Ming-Ming Cheng, Fang-Lue Zhang, Niloy J Mitra, Xiaolei Huang, and Shi-Min Hu. Repfinder: finding approximately repeated scene elements for image editing. *ACM transactions on graphics (TOG)*, 29(4):1–8, 2010.
- [16] Seokju Cho, Sunghwan Hong, Sangryul Jeon, Yunsung Lee, Kwanghoon Sohn, and Seungryong Kim. Cats: Cost aggregation transformers for visual correspondence. *Advances in Neural Information Processing Systems*, 34:9011–9023, 2021.
- [17] Seokju Cho, Sunghwan Hong, and Seungryong Kim. Cats++: Boosting cost aggregation with convolutions and transformers. *IEEE Transactions on Pattern Analysis and Machine Intelligence*, 2022.
- [18] Marius Cordts, Mohamed Omran, Sebastian Ramos, Timo Rehfeld, Markus Enzweiler, Rodrigo Benenson, Uwe Franke, Stefan Roth, and Bernt Schiele. The cityscapes dataset for semantic urban scene understanding. In *Proceedings of the IEEE conference on computer vision and pattern recognition*, pages 3213–3223, 2016.
- [19] Prafulla Dhariwal and Alexander Nichol. Diffusion models beat gans on image synthesis. *NeurIPS*, 34:8780–8794, 2021.
- [20] Alexey Dosovitskiy, Philipp Fischer, Eddy Ilg, Philip Hausser, Caner Hazirbas, Vladimir Golkov, Patrick Van Der Smagt, Daniel Cremers, and Thomas Brox. Flownet: Learning optical flow with convolutional networks. In *Proceedings of the IEEE international conference on computer vision*, pages 2758–2766, 2015.

[21] Marius Drulea and Sergiu Nedevschi. Total variation regularization of local-global optical flow. In *2011 14th International IEEE Conference on Intelligent Transportation Systems (ITSC)*, pages 318–323. IEEE, 2011.

[22] Yiqun Duan, Xianda Guo, and Zheng Zhu. Diffusiondepth: Diffusion denoising approach for monocular depth estimation. *arXiv preprint arXiv:2303.05021*, 2023.

[23] Olivier Duchenne, Armand Joulin, and Jean Ponce. A graph-matching kernel for object categorization. In *2011 International Conference on Computer Vision*, pages 1792–1799. IEEE, 2011.

[24] Hugh Durrant-Whyte and Tim Bailey. Simultaneous localization and mapping: part i. *IEEE robotics & automation magazine*, 13(2):99–110, 2006.

[25] Giorgio Giannone, Didrik Nielsen, and Ole Winther. Few-shot diffusion models. *arXiv preprint arXiv:2205.15463*, 2022.

[26] Dorothy M Greig, Bruce T Porteous, and Allan H Seheult. Exact maximum a posteriori estimation for binary images. *Journal of the Royal Statistical Society: Series B (Methodological)*, 51(2):271–279, 1989.

[27] Zhangxuan Gu, Haoxing Chen, Zhuoer Xu, Jun Lan, Changhua Meng, and Weiqiang Wang. Diffusioninst: Diffusion model for instance segmentation. *arXiv preprint arXiv:2212.02773*, 2022.

[28] Bumsub Ham, Minsu Cho, Cordelia Schmid, and Jean Ponce. Proposal flow. In *Proceedings of the IEEE Conference on Computer Vision and Pattern Recognition*, pages 3475–3484, 2016.

[29] Dan Hendrycks and Thomas Dietterich. Benchmarking neural network robustness to common corruptions and perturbations. In *International Conference on Learning Representations*, 2019.

[30] Jonathan Ho, Ajay Jain, and Pieter Abbeel. Denoising diffusion probabilistic models. *NeurIPS*, 33:6840–6851, 2020.

[31] Karl Holmquist and Bastian Wandt. Diffpose: Multi-hypothesis human pose estimation using diffusion models. *arXiv preprint arXiv:2211.16487*, 2022.

[32] Sunghwan Hong and Seungryong Kim. Deep matching prior: Test-time optimization for dense correspondence. In *Proceedings of the IEEE/CVF International Conference on Computer Vision*, pages 9907–9917, 2021.

[33] Sunghwan Hong, Jisu Nam, Seokju Cho, Susung Hong, Sangryul Jeon, Dongbo Min, and Seungryong Kim. Neural matching fields: Implicit representation of matching fields for visual correspondence. *arXiv preprint arXiv:2210.02689*, 2022.

[34] Berthold K.P. Horn and Brian G. Schunck. Determining optical flow. *Artificial Intelligence*, 17(1):185–203, 1981.

[35] Asmaa Hosni, Christoph Rhemann, Michael Bleyer, Carsten Rother, and Margrit Gelautz. Fast cost-volume filtering for visual correspondence and beyond. *IEEE transactions on pattern analysis and machine intelligence*, 35(2):504–511, 2012.

[36] Yuan-Ting Hu, Jia-Bin Huang, and Alexander G Schwing. Videomatch: Matching based video object segmentation. In *Proceedings of the European conference on computer vision (ECCV)*, pages 54–70, 2018.

[37] Tak-Wai Hui, Xiaou Tang, and Chen Change Loy. Liteflownet: A lightweight convolutional neural network for optical flow estimation. In *Proceedings of the IEEE conference on computer vision and pattern recognition*, pages 8981–8989, 2018.

[38] Andrey Ignatov, Nikolay Kobyshev, Radu Timofte, Kenneth Vanhoey, and Luc Van Gool. Dslr-quality photos on mobile devices with deep convolutional networks. In *Proceedings of the IEEE international conference on computer vision*, pages 3277–3285, 2017.

[39] Yuanfeng Ji, Zhe Chen, Enze Xie, Lanqing Hong, Xihui Liu, Zhaoqiang Liu, Tong Lu, Zhenguo Li, and Ping Luo. Ddp: Diffusion model for dense visual prediction. *arXiv preprint arXiv:2303.17559*, 2023.

[40] Wei Jiang, Eduard Trulls, Jan Hosang, Andrea Tagliasacchi, and Kwang Moo Yi. Cotr: Correspondence transformer for matching across images. In *Proceedings of the IEEE/CVF International Conference on Computer Vision*, pages 6207–6217, 2021.

[41] James Joyce. Bayes’ theorem. 2003.

[42] Tero Karras, Samuli Laine, Miika Aittala, Janne Hellsten, Jaakko Lehtinen, and Timo Aila. Analyzing and improving the image quality of stylegan. In *Proceedings of the IEEE/CVF conference on computer vision and pattern recognition*, pages 8110–8119, 2020.

[43] Gyeongnyeon Kim, Wooseok Jang, Gyuseong Lee, Susung Hong, Junyoung Seo, and Seungryong Kim. Dag: Depth-aware guidance with denoising diffusion probabilistic models. *arXiv preprint arXiv:2212.08861*, 2022.

[44] Jaechul Kim, Ce Liu, Fei Sha, and Kristen Grauman. Deformable spatial pyramid matching for fast dense correspondences. In *Proceedings of the IEEE Conference on Computer Vision and Pattern Recognition*, pages 2307–2314, 2013.

[45] Seungryong Kim, Stephen Lin, Sang Ryul Jeon, Dongbo Min, and Kwanghoon Sohn. Recurrent transformer networks for semantic correspondence. *Advances in neural information processing systems*, 31, 2018.

[46] Seungryong Kim, Dongbo Min, Bumsub Ham, Sangryul Jeon, Stephen Lin, and Kwanghoon Sohn. Fcss: Fully convolutional self-similarity for dense semantic correspondence. In *Proceedings of the IEEE conference on computer vision and pattern recognition*, pages 6560–6569, 2017.

[47] Seungryong Kim, Dongbo Min, Stephen Lin, and Kwanghoon Sohn. Dctm: Discrete-continuous transformation matching for semantic flow. In *Proceedings of the IEEE International Conference on Computer Vision*, pages 4529–4538, 2017.

[48] Claudia Kondermann, Daniel Kondermann, Bernd Jähne, and Christoph Garbe. An adaptive confidence measure for optical flows based on linear subspace projections. In *Pattern Recognition: 29th DAGM Symposium, Heidelberg, Germany, September 12-14, 2007. Proceedings 29*, pages 132–141. Springer, 2007.

[49] Claudia Kondermann, Rudolf Mester, and Christoph S Garbe. A statistical confidence measure for optical flows. *ECCV (3)*, 5304:290–301, 2008.

[50] Jan Kybík and Claudia Nieuwenhuis. Bootstrap optical flow confidence and uncertainty measure. *Computer Vision and Image Understanding*, 115(10):1449–1462, 2011.

[51] Zihang Lai and Weidi Xie. Self-supervised learning for video correspondence flow. *arXiv preprint arXiv:1905.00875*, 2019.

[52] Jae Yong Lee, Joseph DeGol, Victor Fragoso, and Sudipta N Sinha. Patchmatch-based neighborhood consensus for semantic correspondence. In *Proceedings of the IEEE/CVF Conference on Computer Vision and Pattern Recognition*, pages 13153–13163, 2021.

[53] Maxime Lhuillier and Long Quan. Robust dense matching using local and global geometric constraints. In *Proceedings 15th International Conference on Pattern Recognition. ICPR-2000*, volume 1, pages 968–972. IEEE, 2000.

[54] Tsung-Yi Lin, Michael Maire, Serge Belongie, James Hays, Pietro Perona, Deva Ramanan, Piotr Dollár, and C Lawrence Zitnick. Microsoft coco: Common objects in context. In *Computer Vision–ECCV 2014: 13th European Conference, Zurich, Switzerland, September 6–12, 2014, Proceedings, Part V 13*, pages 740–755. Springer, 2014.

[55] Ce Liu, Jenny Yuen, and Antonio Torralba. Sift flow: Dense correspondence across scenes and its applications. *IEEE transactions on pattern analysis and machine intelligence*, 33(5):978–994, 2010.

[56] Ilya Loshchilov and Frank Hutter. Decoupled weight decay regularization. *arXiv preprint arXiv:1711.05101*, 2017.

[57] David G Lowe. Distinctive image features from scale-invariant keypoints. *International journal of computer vision*, 60:91–110, 2004.

[58] Bruce D. Lucas and Takeo Kanade. An iterative image registration technique with an application to stereo vision. In *Proceedings of the 7th International Joint Conference on Artificial Intelligence - Volume 2*, page 674–679, 1981.

[59] Andreas Lugmayr, Martin Danelljan, Andres Romero, Fisher Yu, Radu Timofte, and Luc Van Gool. Repaint: Inpainting using denoising diffusion probabilistic models. In *Proceedings of the IEEE/CVF Conference on Computer Vision and Pattern Recognition*, pages 11461–11471, 2022.

[60] Oisin Mac Aodha, Ahmad Humayun, Marc Pollefeys, and Gabriel J Brostow. Learning a confidence measure for optical flow. *IEEE transactions on pattern analysis and machine intelligence*, 35(5):1107–1120, 2012.

[61] Iaroslav Melekhov, Aleksei Tiulpin, Torsten Sattler, Marc Pollefeys, Esa Rahtu, and Juho Kannala. Dgc-net: Dense geometric correspondence network. In *2019 IEEE Winter Conference on Applications of Computer Vision (WACV)*, pages 1034–1042. IEEE, 2019.

[62] Juhong Min and Minsu Cho. Convolutional hough matching networks. In *Proceedings of the IEEE/CVF Conference on Computer Vision and Pattern Recognition*, pages 2940–2950, 2021.

[63] Juhong Min, Dahyun Kang, and Minsu Cho. Hypercorrelation squeeze for few-shot segmentation. In *Proceedings of the IEEE/CVF international conference on computer vision*, pages 6941–6952, 2021.

[64] Juhong Min, Jongmin Lee, Jean Ponce, and Minsu Cho. Hyperpixel flow: Semantic correspondence with multi-layer neural features. In *Proceedings of the IEEE/CVF International Conference on Computer Vision*, pages 3395–3404, 2019.

[65] Juhong Min, Jongmin Lee, Jean Ponce, and Minsu Cho. Learning to compose hypercolumns for visual correspondence. In *Computer Vision–ECCV 2020: 16th European Conference, Glasgow, UK, August 23–28, 2020, Proceedings, Part XV 16*, pages 346–363. Springer, 2020.

[66] Chong Mou, Xintao Wang, Liangbin Xie, Jian Zhang, Zhongang Qi, Ying Shan, and Xiaohu Qie. T2i-adapter: Learning adapters to dig out more controllable ability for text-to-image diffusion models. *arXiv preprint arXiv:2302.08453*, 2023.

[67] Alex Nichol, Prafulla Dhariwal, Aditya Ramesh, Pranav Shyam, Pamela Mishkin, Bob McGrew, Ilya Sutskever, and Mark Chen. Glide: Towards photorealistic image generation and editing with text-guided diffusion models. *arXiv preprint arXiv:2112.10741*, 2021.

[68] Alexander Quinn Nichol and Prafulla Dhariwal. Improved denoising diffusion probabilistic models. In *ICML*, pages 8162–8171. PMLR, 2021.

[69] David Nistér, Oleg Naroditsky, and James Bergen. Visual odometry. In *Proceedings of the 2004 IEEE Computer Society Conference on Computer Vision and Pattern Recognition, 2004. CVPR 2004.*, volume 1, pages I–I. Ieee, 2004.

[70] Adam Paszke, Sam Gross, Francisco Massa, Adam Lerer, James Bradbury, Gregory Chanan, Trevor Killeen, Zeming Lin, Natalia Gimelshein, Luca Antiga, et al. Pytorch: An imperative style, high-performance deep learning library. *Advances in neural information processing systems*, 32, 2019.

[71] Javier Sánchez Pérez, Enric Meinhardt-Llopis, and Gabriele Facciolo. Tvl1 optical flow estimation. *Image Processing On Line*, 2013:137–150, 2013.

[72] Aditya Ramesh, Prafulla Dhariwal, Alex Nichol, Casey Chu, and Mark Chen. Hierarchical text-conditional image generation with clip latents. *arXiv preprint arXiv:2204.06125*, 2022.

[73] Anurag Ranjan and Michael J Black. Optical flow estimation using a spatial pyramid network. In *Proceedings of the IEEE conference on computer vision and pattern recognition*, pages 4161–4170, 2017.

[74] Jerome Revaud, Philippe Weinzaepfel, Zaid Harchaoui, and Cordelia Schmid. Epicflow: Edge-preserving interpolation of correspondences for optical flow. In *Proceedings of the IEEE conference on computer vision and pattern recognition*, pages 1164–1172, 2015.

[75] Ignacio Rocco, Relja Arandjelovic, and Josef Sivic. Convolutional neural network architecture for geometric matching. In *Proceedings of the IEEE conference on computer vision and pattern recognition*, pages 6148–6157, 2017.

[76] Ignacio Rocco, Mircea Cimpoi, Relja Arandjelović, Akihiko Torii, Tomas Pajdla, and Josef Sivic. Ncnet: Neighbourhood consensus networks for estimating image correspondences. *IEEE Transactions on Pattern Analysis and Machine Intelligence*, 44(2):1020–1034, 2020.

[77] Robin Rombach, Andreas Blattmann, Dominik Lorenz, Patrick Esser, and Björn Ommer. High-resolution image synthesis with latent diffusion models. In *CVPR*, pages 10684–10695, 2022.

[78] Chitwan Saharia, William Chan, Huiwen Chang, Chris Lee, Jonathan Ho, Tim Salimans, David Fleet, and Mohammad Norouzi. Palette: Image-to-image diffusion models. In *ACM SIGGRAPH 2022 Conference Proceedings*, pages 1–10, 2022.

[79] Chitwan Saharia, William Chan, Saurabh Saxena, Lala Li, Jay Whang, Emily Denton, Seyed Kamyar Seyed Ghasemipour, Burcu Karagol Ayan, S Sara Mahdavi, Rapha Gontijo Lopes, et al. Photorealistic text-to-image diffusion models with deep language understanding. *arXiv preprint arXiv:2205.11487*, 2022.

[80] Paul-Edouard Sarlin, Daniel DeTone, Tomasz Malisiewicz, and Andrew Rabinovich. Superglue: Learning feature matching with graph neural networks. In *Proceedings of the IEEE/CVF conference on computer vision and pattern recognition*, pages 4938–4947, 2020.

[81] Saurabh Saxena, Abhishek Kar, Mohammad Norouzi, and David J. Fleet. Monocular depth estimation using diffusion models, 2023.

[82] Johannes L Schonberger and Jan-Michael Frahm. Structure-from-motion revisited. In *Proceedings of the IEEE conference on computer vision and pattern recognition*, pages 4104–4113, 2016.

[83] Thomas Schops, Johannes L Schonberger, Silvano Galliani, Torsten Sattler, Konrad Schindler, Marc Pollefeys, and Andreas Geiger. A multi-view stereo benchmark with high-resolution images and multi-camera videos. In *Proceedings of the IEEE Conference on Computer Vision and Pattern Recognition*, pages 3260–3269, 2017.

[84] Junyoung Seo, Gyuseong Lee, Seokju Cho, Jiyoung Lee, and Seungryong Kim. Midms: Matching interleaved diffusion models for exemplar-based image translation. 2023.

[85] Tianwei Shen, Lei Zhou, Zixin Luo, Yao Yao, Shiwei Li, Jiahui Zhang, Tian Fang, and Long Quan. Self-supervised learning of depth and motion under photometric inconsistency. In *Proceedings of the IEEE/CVF International Conference on Computer Vision Workshops*, pages 0–0, 2019.

[86] Eero P Simoncelli, Edward H Adelson, and David J Heeger. Probability distributions of optical flow. In *CVPR*, volume 91, pages 310–315, 1991.

[87] Karen Simonyan and Andrew Zisserman. Very deep convolutional networks for large-scale image recognition. *arXiv preprint arXiv:1409.1556*, 2014.

[88] Jascha Sohl-Dickstein, Eric Weiss, Niru Maheswaranathan, and Surya Ganguli. Deep unsupervised learning using nonequilibrium thermodynamics. In *ICML*, pages 2256–2265. PMLR, 2015.

[89] Jiaming Song, Chenlin Meng, and Stefano Ermon. Denoising diffusion implicit models. *arXiv preprint arXiv:2010.02502*, 2020.

[90] Yang Song and Stefano Ermon. Generative modeling by estimating gradients of the data distribution. *NeurIPS*, 32, 2019.

[91] Yang Song, Jascha Sohl-Dickstein, Diederik P Kingma, Abhishek Kumar, Stefano Ermon, and Ben Poole. Score-based generative modeling through stochastic differential equations. In *ICLR*, 2020.

[92] Deqing Sun, Stefan Roth, and Michael J Black. Secrets of optical flow estimation and their principles. In *2010 IEEE computer society conference on computer vision and pattern recognition*, pages 2432–2439. IEEE, 2010.

[93] Deqing Sun, Stefan Roth, John P Lewis, and Michael J Black. Learning optical flow. In *Computer Vision–ECCV 2008: 10th European Conference on Computer Vision, Marseille, France, October 12–18, 2008, Proceedings, Part III 10*, pages 83–97. Springer, 2008.

[94] Deqing Sun, Xiaodong Yang, Ming-Yu Liu, and Jan Kautz. Pwc-net: Cnns for optical flow using pyramid, warping, and cost volume. In *Proceedings of the IEEE conference on computer vision and pattern recognition*, pages 8934–8943, 2018.

[95] Tatsunori Taniai, Sudipta N Sinha, and Yoichi Sato. Joint recovery of dense correspondence and cosegmentation in two images. In *Proceedings of the IEEE conference on computer vision and pattern recognition*, pages 4246–4255, 2016.

[96] Zachary Teed and Jia Deng. Raft: Recurrent all-pairs field transforms for optical flow. In *Computer Vision–ECCV 2020: 16th European Conference, Glasgow, UK, August 23–28, 2020, Proceedings, Part II 16*, pages 402–419. Springer, 2020.

[97] Guy Tevet, Sigal Raab, Brian Gordon, Yonatan Shafir, Daniel Cohen-Or, and Amit H Bermano. Human motion diffusion model. *arXiv preprint arXiv:2209.14916*, 2022.

[98] Prune Truong, Martin Danelljan, Luc V Gool, and Radu Timofte. Gocor: Bringing globally optimized correspondence volumes into your neural network. *Advances in Neural Information Processing Systems*, 33:14278–14290, 2020.

[99] Prune Truong, Martin Danelljan, and Radu Timofte. Glu-net: Global-local universal network for dense flow and correspondences. In *Proceedings of the IEEE/CVF conference on computer vision and pattern recognition*, pages 6258–6268, 2020.

[100] Prune Truong, Martin Danelljan, Luc Van Gool, and Radu Timofte. Learning accurate dense correspondences and when to trust them. In *Proceedings of the IEEE/CVF Conference on Computer Vision and Pattern Recognition*, pages 5714–5724, 2021.

[101] Benjamin Ummenhofer, Huizhong Zhou, Jonas Uhrig, Nikolaus Mayer, Eddy Ilg, Alexey Dosovitskiy, and Thomas Brox. Demon: Depth and motion network for learning monocular stereo. In *Proceedings of the IEEE conference on computer vision and pattern recognition*, pages 5038–5047, 2017.

[102] Anne S Wannenwetsch, Margret Keuper, and Stefan Roth. Probflow: Joint optical flow and uncertainty estimation. In *Proceedings of the IEEE international conference on computer vision*, pages 1173–1182, 2017.

[103] Philippe Weinzaepfel, Jerome Revaud, Zaid Harchaoui, and Cordelia Schmid. Deepflow: Large displacement optical flow with deep matching. In *Proceedings of the IEEE international conference on computer vision*, pages 1385–1392, 2013.

[104] Manuel Werlberger, Thomas Pock, and Horst Bischof. Motion estimation with non-local total variation regularization. In *2010 IEEE Computer Society Conference on Computer Vision and Pattern Recognition*, pages 2464–2471. IEEE, 2010.

[105] Lvmi Zhang and Maneesh Agrawala. Adding conditional control to text-to-image diffusion models. *arXiv preprint arXiv:2302.05543*, 2023.

[106] Pan Zhang, Bo Zhang, Dong Chen, Lu Yuan, and Fang Wen. Cross-domain correspondence learning for exemplar-based image translation. In *Proceedings of the IEEE/CVF Conference on Computer Vision and Pattern Recognition*, pages 5143–5153, 2020.

[107] Bolei Zhou, Hang Zhao, Xavier Puig, Tete Xiao, Sanja Fidler, Adela Barriuso, and Antonio Torralba. Semantic understanding of scenes through the ade20k dataset. *International Journal of Computer Vision*, 127:302–321, 2019.

Appendix

A More implementation details

A.1 Details of conditional denoising diffusion module

Our conditional denoising diffusion module is formally based on Improved DDPM [68], except for some modifications. Specifically, we modified the input channel dimension to include additional conditions D_{src} and F_{init} , along with the noisy matching field F_t . The training images were resized to the resolution of 512×512 . We extracted hierarchical feature maps with dimensions of 16×16 , 32×32 , and 64×64 , following the protocol in [99, 98]. The dimensions of F_t , D_{tgt} , and F_{init} were set to 64×64 . F_{init} is derived from the sum of all correlation levels and a soft-argmax operation [16].

A.2 Details of cost injection module

We computed 4D correlation volumes $C \in \mathbb{R}^{b_{\text{src}}^l \times w_{\text{src}}^l \times h_{\text{tgt}}^l \times w_{\text{tgt}}^l}$ from each l -th level of feature resolutions, and each correlation volume subsequently passes through its corresponding cost embedding layer. The cost embedding layer comprises 4D convolutions, Group Normalization, and the ReLU operation. Within the 4D convolutions, large strides periodically reduce the last two target spatial dimensions of the correlation map to $(1, 1)$, while the first two source spatial dimensions remain unchanged. The following processes are explained in Sec 4.3 of the main paper.

A.3 Training details

Our baseline code is developed based on the DenseMatching repository¹. We implemented the network using PyTorch [70] and trained it with the AdamW optimizer [56] with a learning rate of $1e^{-4}$ in the first stage and $3e^{-5}$ in the second stage. In the first stage, we trained the denoising diffusion module with 100,000 iterations using a batch size of 18, while in the second stage, we trained the cost injector module with 10,000 iterations and a batch size of 4. During training, we set the diffusion time step T to 4,000. All experiments were conducted using 6 24GB RTX 3090 GPUs.

A.4 Inference details

We employ the DDIM sampler [89] for diffusion reverse sampling, setting the diffusion time step to 5. Empirically, we discovered that the proposed reinitialization technique is particularly effective when the correspondence error of F_{init} is significantly large. For an effective trade-off between inference speed and performance, we controlled the reinitialization technique by computing cycle consistency error [4] between forward and backward matching. If the cycle consistency error is lower than threshold $\tau = 0.2$, we stop the recursion process. In addition, we set the limitation of iteration to 200. It is noteworthy that the average number of iterations on HPatches [3] is 7, which is much lower than the 300 in DMP [32].

A.5 Evaluation datasets

We evaluated DiffMatch on standard geometric matching benchmarks: HPatches [3] and ETH3D [83]. To further investigate the effectiveness of the diffusion generative prior, we also evaluated DiffMatch under the harshly corrupted settings [29] of HPatches [3] and ETH3D [83]. Here, we provide detailed information about these datasets.

HPatches. We evaluated our method on the challenging HPatches dataset [3], consisting of 59 image sequences with geometric transformations and significant viewpoint changes. The dataset contains images with resolutions ranging from 450×600 to $1,613 \times 1,210$.

ETH3D. We evaluated our framework on the ETH3D dataset [83], which consists of multi-view indoor and outdoor scenes with transformations not constrained to simple homographies. ETH3D comprises images with resolutions ranging from 480×752 to 514×955 and consists of 10 image sequences. For a fair comparison, we followed the protocol of [99], which collects pairs of images at different intervals. We selected approximately 500 image pairs from these intervals.

¹DenseMatching repository: <https://github.com/PruneTruong/DenseMatching>.

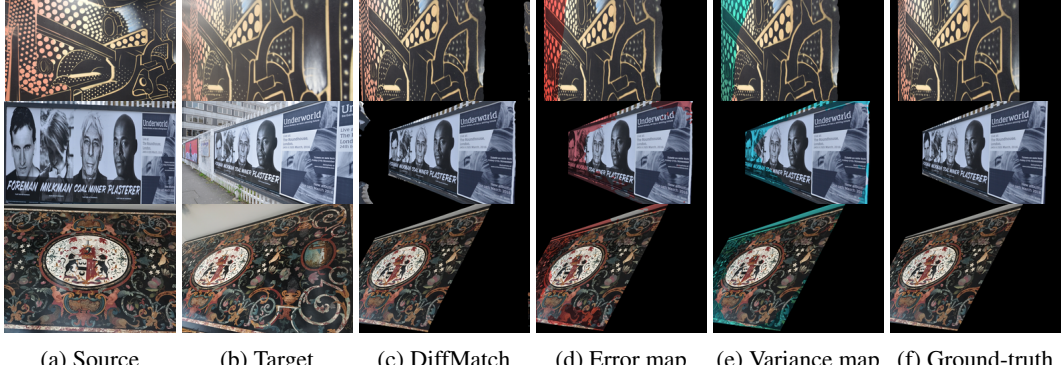


Figure 8: **Uncertainty estimation:** Our framework can measure the pixel-wise mean and variance of estimated matching fields by sampling from different Gaussian noises. We observe that the variance maps are formed almost the same as the error map, which shows that our variance map successfully expresses the uncertainty of dense correspondence.

Corruptions. In the evaluation on ETH3D [83], we observed that DiffMatch sometimes exhibits poor performance in intervals with small displacements. However, models designed for optical flow, such as PWCNet [94], RAFT [96], GLU-Net [99] and GLU-Net-GOCOR [98], demonstrate relatively high performance in small displacements by leveraging local correlation to find the exact matching point within a local region. This finding directly contradicts our research objective, which aims to design a powerful generative prior capable of handling the inherent ambiguities in dense correspondence tasks, including textureless regions, repetitive patterns, and large displacements.

To this end, to evaluate the robustness of our generative prior on more challenging datasets, we applied a set of common corruptions introduced in ImageNet-C [29]. This corruption consists of 15 types of algorithmically generated corruptions, which are grouped into four distinct categories: noise, blur, weather, and digital. Each corruption type includes five different severity levels, resulting in a total of 75 unique corruptions. For our evaluation, we specifically selected severity level 5 to highlight the effectiveness of our generative prior. Here, we provide detailed information about each of the corruptions.

Gaussian noise is a specific type of random noise that typically arises in low-light conditions. Shot noise, also known as Poisson noise, is an electronic noise that originates from the inherent discreteness of light. Impulse noise, a color analogue of salt-and-pepper noise, occurs due to bit errors within an image. Defocus blur occurs when an image is out of focus, causing a loss of sharpness. Frosted glass blur is commonly seen on frosted glass surfaces, such as panels or windows. Motion blur arises when the camera moves rapidly, while zoom blur occurs when the camera quickly zooms towards an object. Snow, a type of precipitation, can cause visual obstruction in images. Frost, created when ice crystals form on lenses or windows, can obstruct the view. Fog, which conceals objects and is usually rendered using the diamond-square algorithm, also affects visibility. Brightness is influenced by daylight intensity. Contrast depends on lighting conditions and the color of an object. Elastic transformations apply stretching or contraction to small regions within an image. Pixelation arises when low-resolution images undergo upsampling. JPEG, a lossy image compression format, introduces artifacts during image compression.

B Additional analyses

B.1 Uncertainty estimation

Interestingly, DiffMatch naturally derives the uncertainty of estimated matches by taking advantage of the inherent stochastic property of a generative model. We accomplish this by calculating the pixel-level variance in generated samples across various initializations of Gaussian noise F_T . On the other hand, it is crucial to determine when and where to trust estimated matches in dense correspondence [100, 49, 60, 8, 50, 102, 101]. Earlier approaches [48, 49, 60] relied on post-hoc techniques to assess the reliability of models, while more recent model-inherent approaches [100, 8, 50, 102, 101] have developed frameworks specifically designed for uncertainty estimation. The

Table 6: **Quantitative evaluation on HPatches [3] and ETH3D [83] with common corruptions from ImageNet-C [29].** All results are evaluated at corruption severity 5. For simplicity, we denote raw correlation volume and GLU-Net-GOCor as Raw corr. and GOCor [98], respectively. We additionally report the matching performance of the raw correlation volume to demonstrate the effect of our proposed generative matching prior.

Dataset	Algorithm	Gauss.	Noise	Shot	Impulse	Defocus	Blur	Glass	Motion	Zoom	Snow	Frost	Fog	Bright	Contrast	Digital	Elastic	Pixel	JPEG	Avg.
HPatches [3]	Raw corr.	156.5	149.6	153.5	104.0	94.26	244.3	176.9	227.8	254.4	222.1	104.6	141.6	116.5	197.5	131.5	165.0			
	GLU-Net [99]	34.96	32.60	34.18	25.74	25.71	63.26	90.75	46.16	66.63	47.81	25.28	37.45	32.85	44.31	26.94	42.31			
	GOCor [98]	27.35	27.21	26.63	23.54	20.75	57.75	88.35	39.84	63.55	36.98	21.44	23.65	28.40	33.67	22.20	36.09			
	DiffMatch	30.82	29.18	29.73	21.76	19.21	56.87	95.06	35.48	48.24	31.10	19.33	27.41	28.00	35.57	23.68	35.42			
ETH3D [83]	Raw corr.	103.3	94.97	102.3	41.78	36.31	141.3	135.4	153.9	177.7	140.0	50.06	60.16	62.61	95.78	63.97	97.30			
	GLU-Net [99]	29.20	27.51	29.11	14.18	13.16	36.90	77.73	47.11	65.22	37.75	13.89	24.52	19.11	21.25	17.77	31.63			
	GOCor [98]	27.45	25.56	26.44	11.39	10.98	33.73	73.56	43.24	66.49	39.11	10.98	18.34	15.54	16.47	15.20	28.96			
	DiffMatch	26.40	23.63	26.17	8.82	7.66	34.01	69.30	38.99	64.82	26.93	10.04	15.17	13.89	17.37	15.39	26.57			

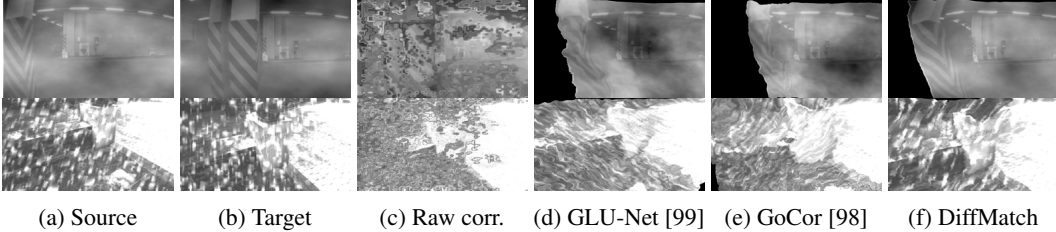


Figure 9: **Visualizing the effectiveness of the proposed generative matching prior:** The input images are corrupted by fog and snow corruptions (top and bottom, respectively). Compared to raw correlation and previous methods [99, 98] that focus solely on point-to-point feature relationships, our approach yields more natural and precise matching results by effectively learning the matching field manifold.

trustworthiness of this uncertainty is showcased in Fig. 8. We found a direct correspondence between highly erroneous locations and high-variance locations, emphasizing the potential to interpret the variance as uncertainty. We believe this provides promising opportunities for applications demanding high reliability, such as medical imaging [1] and autonomous driving [69, 13].

B.2 The effectiveness of generative matching prior

DiffMatch effectively learns the matching manifold and finds natural and precise matches. In contrast, the raw correlation volume, which is computed by dense scalar products between the source and target descriptors, fails to find accurate point-to-point feature relationships in inherent ambiguities in dense correspondence, including repetitive patterns, textureless regions, and large displacements. To highlight the effectiveness of our generative matching prior, we compare the matching performance evaluated by raw correlation and our method under harshly corrupted settings in Table 6 and Fig. 9.

The corruptions introduced by [29] contain the inherent ambiguities in dense correspondence. For instance, snow and frost corruptions obstruct the image pairs by creating repetitive patterns, while fog and brightness corruptions form homogeneous regions. Under these conditions, raw correlation volume fails to find precise point-to-point feature relationships. Conversely, our method effectively finds natural and exact matches within the learned matching manifold, even under severely corrupted conditions. These results highlight the efficacy of our generative prior, which learns both the likelihood and the matching prior, thereby finding the natural matching field even under extreme corruption.

C Additional results

C.1 More qualitative comparison on HPatches and ETH3D

We provide a more detailed comparison between our method and other state-of-the-art methods on HPatches [3] in Fig. 10 and ETH3D [83] in Fig. 11.

C.2 More qualitative comparison in corrupted settings

We also present a qualitative comparison on corrupted HPatches [3] and ETH3D [83] in Fig. 12 and Fig. 13, respectively.

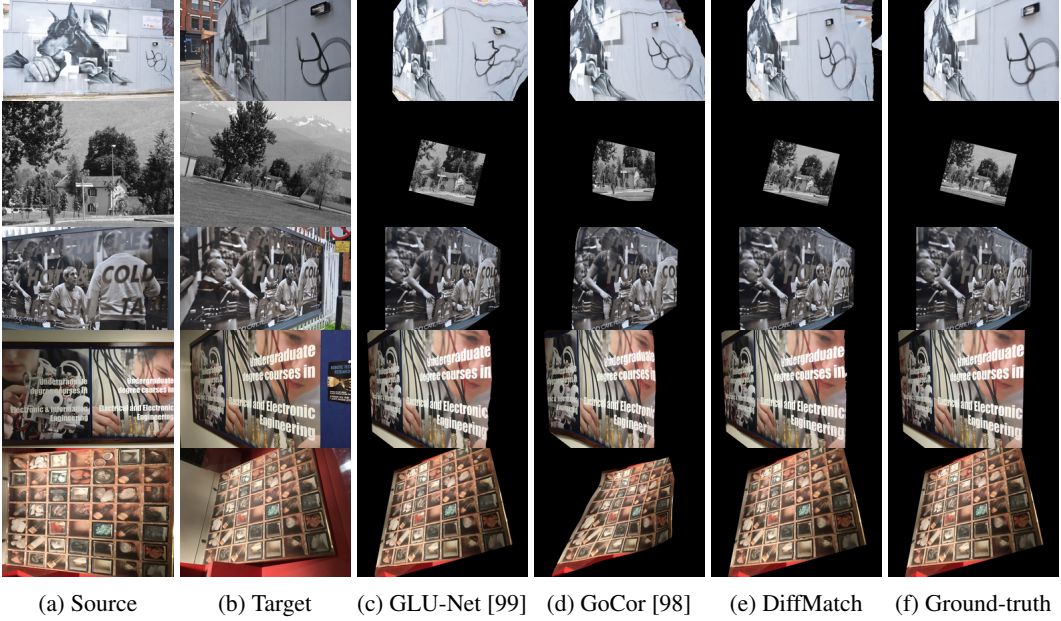


Figure 10: **Qualitative results on HPatches [83]:** the source images are warped to the target images using predicted correspondences.

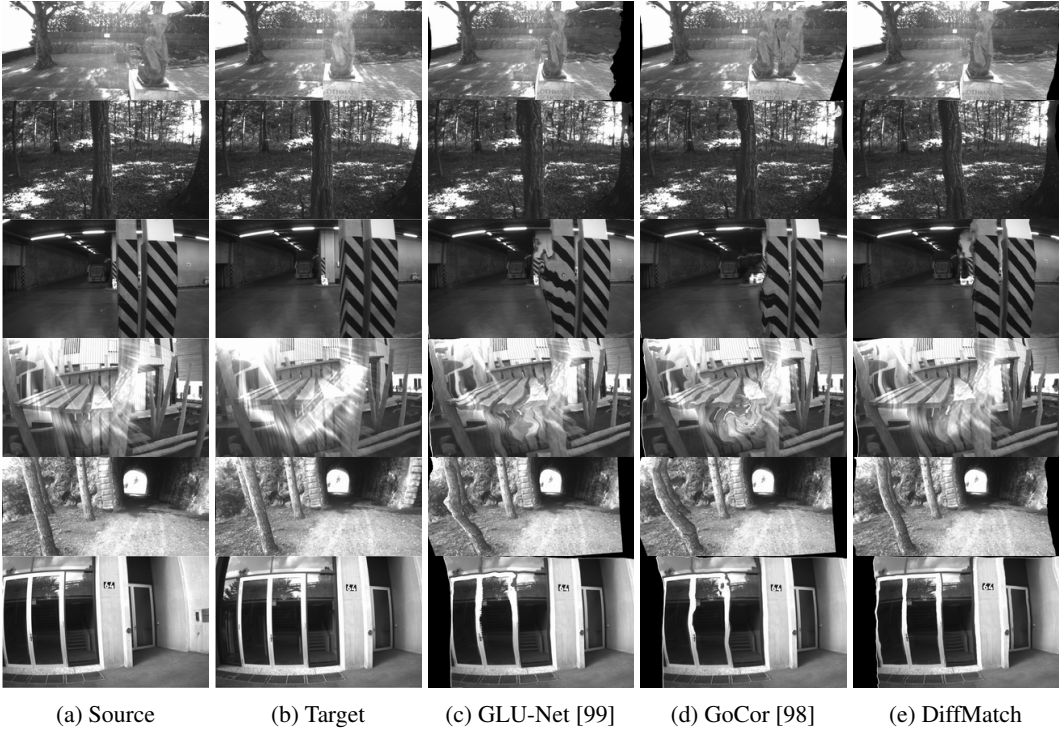


Figure 11: **Qualitative results on ETH3D [83]:** the source images are warped to the target images using predicted correspondences.

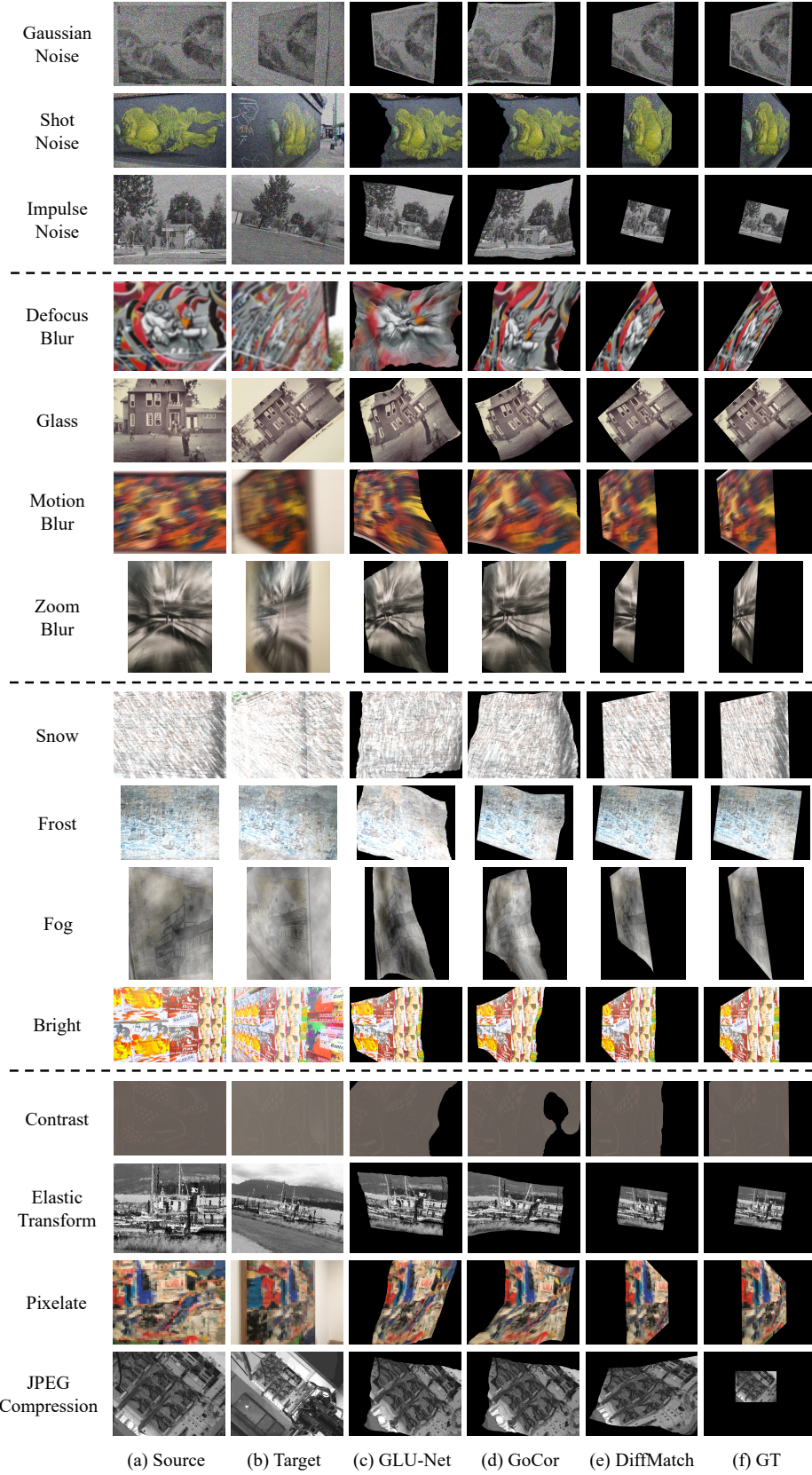


Figure 12: **Qualitative results on HPatches [83] using corruptions in [29]:** the source images are warped to the target images using predicted correspondences.

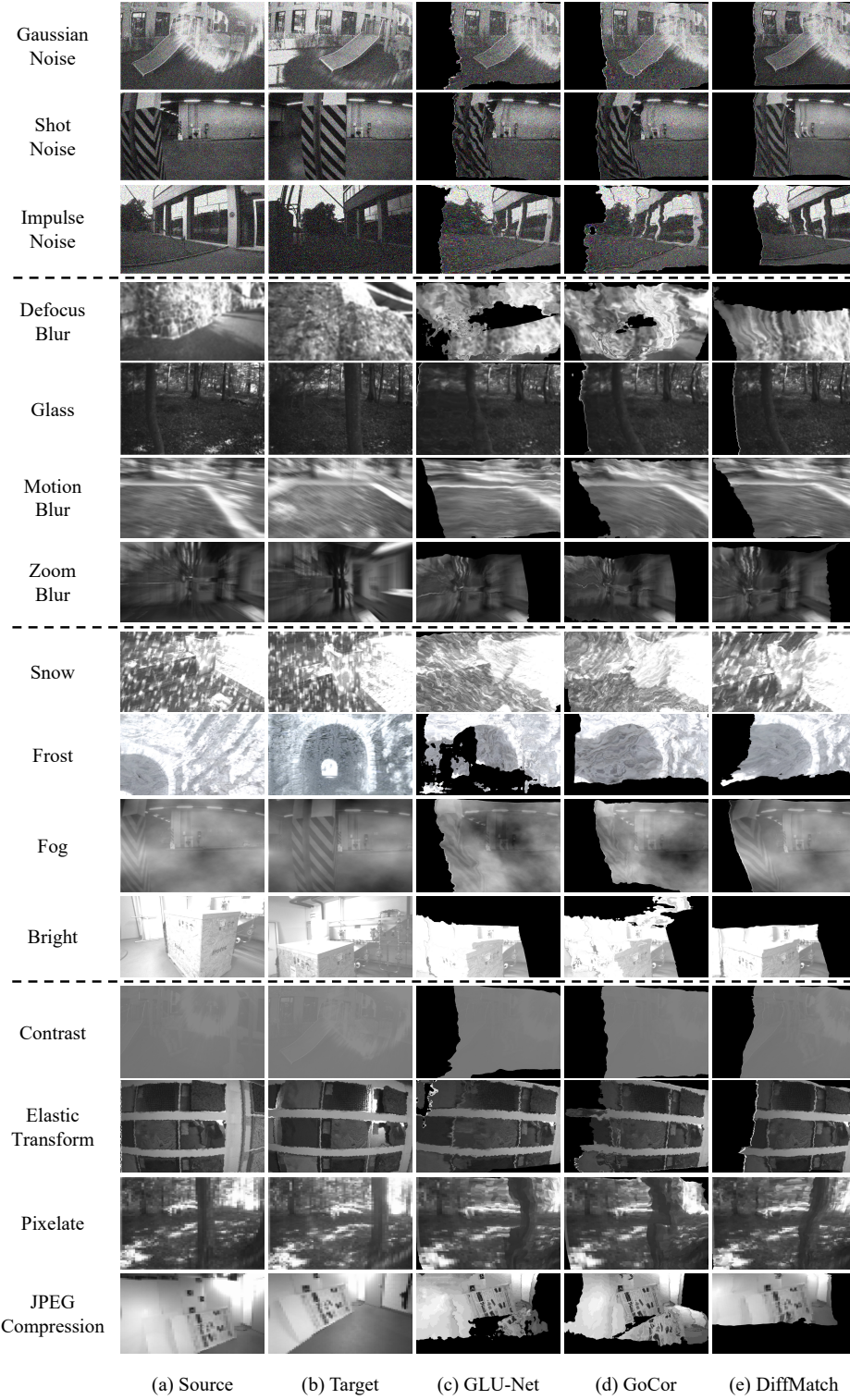


Figure 13: **Qualitative results on ETH3D [83] using corruptions in [29]:** the source images are warped to the target images using predicted correspondences.

D Limitations and future work

To the best of our knowledge, we are the first to formulate the dense correspondence task using a generative approach. We have demonstrated the importance of learning the manifold of matching fields in dense correspondence through various experiments. However, our method exhibits slightly lower performance on ETH3D [83] during intervals with small displacement. We conjecture that this problem might be mitigated by certain architectural designs and inference techniques aiming to find detailed dense correspondence, such as local correlation [96, 99, 98], flow upsample [33, 96], zoom-in [40], and patch-match techniques [5, 52]. In this work, our primary focus was to demonstrate the importance of learning matching prior with a generative approach and its capacity to cope with harsh conditions for the first time.

In future work, we aim to improve the quality of generated dense correspondence by leveraging more powerful feature extractors than VGG-16 [87]. We will also consider improving our architectural designs and inference techniques to capture the matches with greater accuracy.

E Broader impact

Dense correspondence applications have diverse uses, including simultaneous localization and mapping (SLAM) [24, 2], structure from motion (SfM) [82], image editing [5, 15, 106], and video analysis [36, 51]. Although there is no inherent misuse of dense correspondence, it can be inappropriately used in image editing to produce doctored images of real people. Such misuse of our techniques presents societal problems, and we strongly discourage the use of our work as a means of disseminating false information or damaging our reputation.